Nanoscale Insights: Exploring Undersaturated Crystallisation of Flufenamic Acid with Liquid Phase Transmission Electron Microscopy- Supplementary Information

Sara Fatima[1,3], Junbeom Park[4], Govind Ummethala[5], Shibabrata Basak[4], Rüdiger-A. Eichel[4], Amir Tavabi[5], Rafal Dunin Borkowski[5], Sarah Hudson[1,3], Jennifer Cookman[1,2,3].*

[1] Department of Chemical Sciences, University of Limerick, Limerick, V94 T9PX, Ireland.

[2] Department of Physics, University of Limerick, Limerick, V94 T9PX, Ireland.

[3] SSPC the Research Ireland Centre for Pharmaceuticals, Bernal Institute, University of Limerick, Limerick, V94 T9PX, Ireland

[4] Institute of Energy Technologies - Fundamental Electrochemistry (IET-1), Forschungszentrum Jülich GmbH, 52428 Jülich, Germany.

[5] Ernst-Ruska Centre for Microscopy and Spectroscopy with Electrons, Forschungszentrum Jülich GmbH, 52428 Jülich, Germany.

*Correspondence: Jennifer.Cookman@ul.ie

Table of Contents

S1. Electron Flux Density Quantification

The Gatan K2 Summit direct electron detector was setup in counting mode to calibrate the settings required for the selected electron dose range so that image and video recording could be completed using the 4k x 4k Gatan OneView CMOS camera for improved contrast and manageable framerate. The exact number of electrons striking the material in a specific location was determined using the counted mode of the K2 Summit Direct Electron Detector to estimate the electron flux ($e^-/Å^2/s$) as mentioned in Table S1. The table outlines the calibration parameters adjusted on the K2 detector in order to accurately determine the dose rate corresponding to imaging conditions used on the OneView camera. Given the differences in detector sensitivity, pixel size, and readout architecture between the two systems, a reliable cross-calibration was necessary to ensure consistent and quantitative dose measurements. Parameters such as exposure time, beam current, spot size, and magnification were systematically varied during calibration. These adjustments enabled precise estimation of the

electron flux reaching the sample during OneView acquisitions, which is critical for these dose-sensitive experiments.

Table S1. Parameters changed for calibrations on the K2 to measure the exact dose rate to be used on the OneView.

K2 electron dose ($e^-/Å^2$)	Monochromat-or value	Beam diameter (µm)	Fluscreen electron flux ($e^-/Å^2/s$)	Screen current (nA)	K2 electron flux ($e^-/Å^2/s$)	Magnific-ation
0.100	108	6.01	0.32	0.435	1	9800x
0.200	78.8	6.01	0.59	0.812	2	9800x
0.504	51.77	6.01	1.48	2.05	5	9800x
0.972	17.34	3.39	7.39	10.1	10	9800x
0.103	240.72	2.28	0.38	0.072	1	27000x
0.202	168.05	2.28	0.63	0.118	2	27000x
0.501	102.51	2.28	1.39	0.262	5	27000x
1.004	71.40	2.28	2.65	0.512	10	27000x
5.001	33.92	2.28	13.3	2.51	50	27000x

S2. TEM Calibration

The TEM was operated at an acceleration voltage of 300 kV, spot size 4, C2 aperture was set at 150 µm and the monochromator was centred with respect to the beam position and expanded to minimise the incident electron dose. A gold calibration standard i.e., a thin carbon-film with gold islands, was loaded in the single-tilt holder and basic calibrations of the TEM were performed. After the calibration specimen was inserted, eucentric height was adjusted. A series

of calibrations of the beam position, beam tilt in x and y, positioning of the C2 and C3 apertures and rotation centre was completed at magnification intervals between 2500x and 1.1 Mx. Finally, the stigmatism for the objective and condenser apertures were observed and adjusted to minimise the aberrations. Once completed, the magnification was returned to the 2500x, and the stage reset in preparation for removing the holder.

S3. Polymorph information for FFA

The table below presents the nine reported polymorphs of flufenamic acid (FFA) as described in literature, highlighting their diverse crystal habits and the range of crystallisation techniques employed for their isolation. Each polymorph has been obtained under different experimental conditions, often involving specific solvents, additives, or excipients that influence nucleation and growth pathways. Techniques such as solvent evaporation, cooling crystallisation, sublimation, and mechanochemistry have been used in various studies to stabilise and isolate distinct forms. The accompanying details provide insights into the role of crystallisation environment in directing polymorphic outcome, underscoring the complexity of FFA's solid-state landscape and its sensitivity to subtle changes in crystallisation parameters.

Table S2. The nine reported polymorphs of FFA, as described in literature, including their crystal habits, solvents and excipients used along with the crystallisation techniques.

Polymorph (Form)	**Crystal Habit**	**Solvent**	**Crystallisation Technique**	**Excipients**
Form I[1]	Needles	Toluene, Ethanol	Melt recrystallisation, slow evaporation	None

Form II[2]	Plates	Various (with polymers)	Polymer-induced heteronucleation (PIHn)	Polymer heteronucleant
Form III[3]	Needles (yellow)	Ethanol	Slow cooling/evaporation	None
Form IV[4]	Prisms	None (from amorphous)	Recrystallisation from amorphous dispersion	Trehalose
Form V[2]	Prisms	Ethanol–Water	Salt-induced solution crystallisation	Inorganic salts
Form VI[2]	Not specified	None	Solid–solid phase transition	None
Form VII[2]	Needles	Various	Polymer-induced heteronucleation	Polymer heteronucleant
Form VIII[2]	Plates	Various	Solution crystallisation	None
Form IX[1,5]	Needles	None	Low-temp solid–solid transition	None

S4. Solubility equations

Gravimetric solubility (C_s) of FFA in each solvent was determined using Equation 1, based on the mass of dried solute and the total mass of the solution. Mole fraction solubility ($^{\chi}_{eq}$) was subsequently calculated using Equation 2, incorporating the molecular weights of the solute (FFA) and the respective solvent. These values were used to assess the degree of undersaturation for each experimental condition.

Gravimetric solubility (C_s) was determined using the equation:

$$C_s\,(g/g) = (m_{dry} - m_{empty})/(m_{solution} - m_{dry}) \quad \textit{Equation S1}$$

Mole fraction solubility (x_{eq}) was calculated as:

$$x_{eq} = (Cs * M_2)/(Cs * M_2 + M_1)$$ *Equation S2*

where M_1 and M_2 represent the molecular weights (g/mol) of the solute and solvent, respectively.

S5. Characterisation

1.1. Optical and SEM from Cooling Crystallisation

Methodology of cooling crystallisation: The required amount of API, based on solubility data, was dissolved in the selected solvent to achieve saturation at 313.15 K. The mixture was sealed in a vial and heated to 323.15 K to ensure complete dissolution. Once saturated, the solution was removed from heat and cooled in a water bath at a controlled rate of 1 K/min until reaching the target crystallisation temperature (refer to **Table S3**). The solution was left undisturbed overnight to allow complete crystallisation. Once crystal formation was substantial, vacuum filtration was performed using a 0.2 μm PTFE filter paper in a funnel to separate the solid from the mother liquor. The collected crystals were air-dried at room temperature to prevent degradation. The crystalline habit and purity were analysed using X-ray diffraction (XRD), and crystal morphology was imaged via an Olympus BX51 polarised light optical microscope (PLM).

Table S3. Flufenamic acid supersaturations (S) at the targeted cooling temperatures in different.

API	Solvent	Target cooling temp. (K)	S

FFA	Ethanol	288.15	1.30
	Methanol	283.15	1.15
	Isopropanol	283.15	1.04

Supplementary Figure S2. Optical microscopy and scanning electron microscopy (SEM) images of FFA crystals formed from ethanol (EtOH, top) and isopropanol (IPA, bottom). Optical images were taken at 20× (EtOH) and 10× (IPA) magnification. SEM images were acquired using a Hitachi SU70 at 10.0 kV (EtOH) and 5.0 kV (IPA), with scale bars of 400 µm and 50 µm, respectively. Crystallisation using EtOH typically yields elongated, well-defined crystals, whereas crystallisation with IPA tends to result in thinner, needle-like crystals that are more densely distributed. These variations illustrate the solvent-dependent influence on crystal size, habit, and nucleation behaviour.

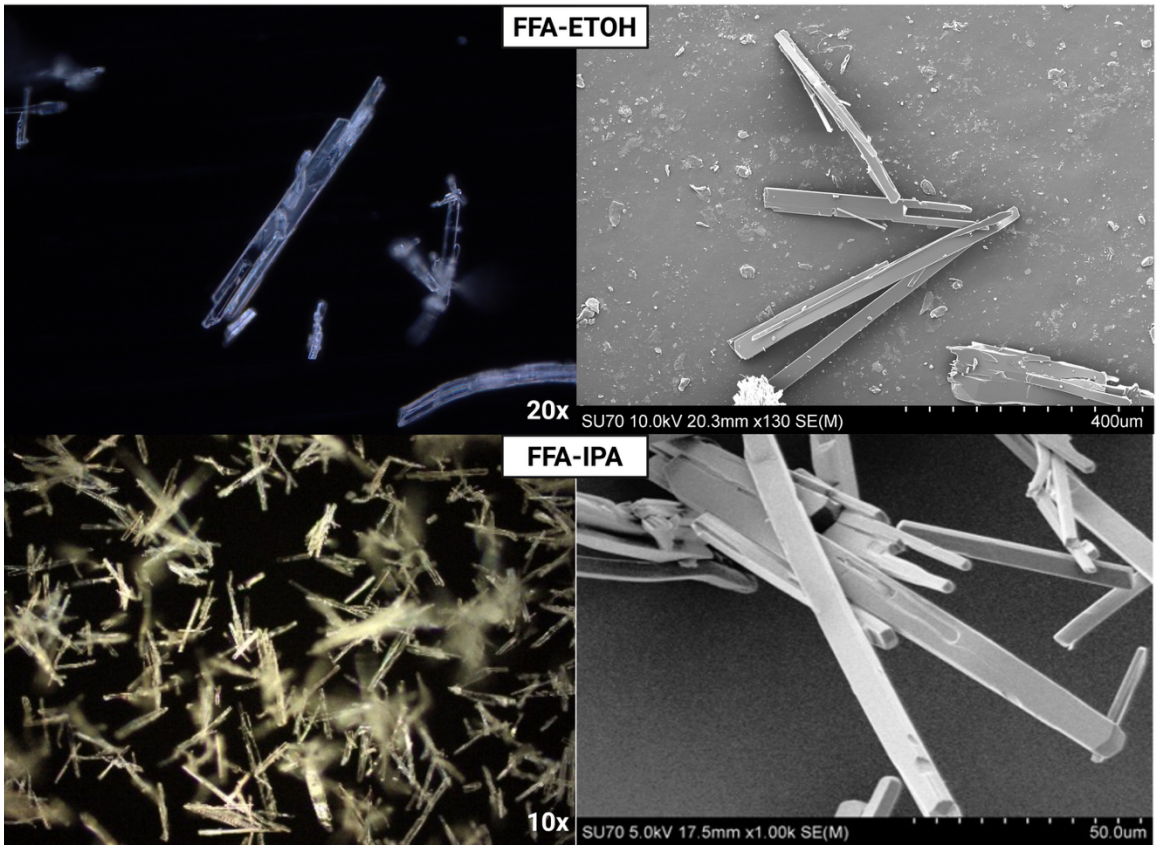

Figure S1. Optical microscopy (left) and SEM (right) images of FFA crystals obtained via cooling crystallisation from ethanol (EtOH) and isopropanol (IPA), depicting the needle like morphology resembling Form III.

1.2. PXRD

Supplementary Figure S2. PXRD patterns of FFA crystallised from the selected solvents in a cooling crystallisation process - IPA, EtOH, and as received (AR), compared against reference patterns for Form I (kinetically stable) and Form III (thermodynamically stable). The diffraction profiles confirm the polymorphic identity of the crystallised samples and enable direct comparison of solvent effects on polymorph selection. The consistent alignment with Form III in different solvents highlights solvent-specific crystallisation behaviour alongside the as-received Form I.

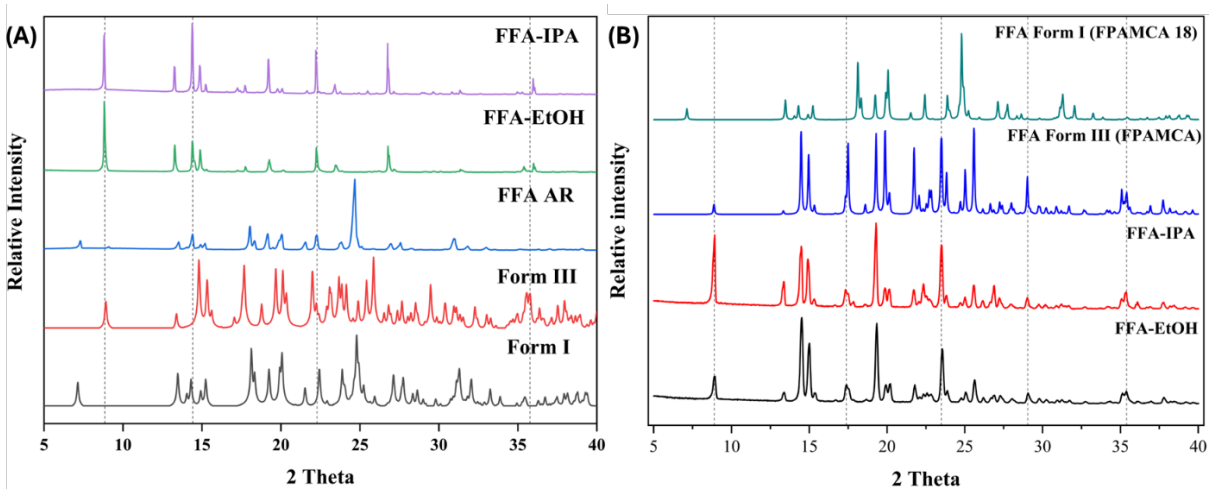

Figure S2. PXRD patterns of FFA crystallised from various screened solvents using the cooling crystallisation technique, compared against reference patterns of the known kinetically (form I) and thermodynamically (form III) stable polymorphic forms. (A) Comparison of all patterns with the as-received sample; (B) Specific comparison of form I and form III with crystals obtained from IPA and EtOH.

S6. LPTEM

1.3. Electron flux modulation- Solvent displacement

Video S1. LPTEM *in situ* recording of solvent displacement from the viewing window upon electron flux >10 $e^{-}/Å^{2}/s$. Rapid bubble formation and thinning of liquid layer are observed, indicating evaporation driven by beam-induced heating and radiolysis. System: FFA-EtOH.

Video S2 and S3. LPTEM video capturing a marked contrast shift as the solvent exits the viewing window at electron flux >10 $e^{-}/Å^{2}/s$. The disappearance of the liquid phase is evidenced by increased image sharpness and reduced dynamic scattering, confirming solvent loss due to beam exposure.

Control test with pure blank solvents

To ensure that the observed nucleation events required the FFA solutions and not caused by the solvent itself, the solvent alone was subjected to continuous irradiation at the tested EFDs for >5 min.

1.4. LPTEM Crystallisation

FFA-ETOH

Video S4 (10 mM). LPTEM video capturing multiple crystal growth events in a 10 mM FFA solution in EtOH under an electron flux of 1 $e^{-}/Å^{2}/s$.

Video S5 (100 mM). LPTEM video capturing crystal growth in a 100 mM FFA solution in EtOH under an electron flux of 1 $e^{-}/Å^{2}/s$. The video shows the dynamic nucleation and growth processes occurring within the solution under continuous electron irradiation.

Video S9 (1 mM). LPTEM video showing the movement of low-concentration clusters in a 1 mM FFA solution in EtOH under an electron flux of 1 $e^{-}/Å^{2}/s$. The video captures the dynamic behaviour and mobility of small aggregates over time under continuous electron irradiation.

Video S10 (1 mM). LPTEM video showing the interaction of low-concentration clusters in a 1 mM FFA solution in EtOH under an electron flux of 1 $e^{-}/Å^{2}/s$. The video captures two clusters approaching and joining over time under continuous electron irradiation.

FFA-IPA

Video S6 (20 mM). LPTEM video showing the nucleation of a 20 mM FFA solution in IPA under an electron flux of 10 $e^{-}/Å^{2}/s$. The video shows nucleation and crystal growth under continuous electron beam irradiation.

Video S7 (15 mM). LPTEM video showing the nucleation of a 15 mM FFA solution in IPA under an electron flux of 10 $e^{-}/Å^{2}/s$. The video shows nucleation and crystal growth under continuous electron beam irradiation.

Video S8 (10 mM). LPTEM video showing the nucleation of a 10 mM FFA solution in IPA under an electron flux of 10 $e^{-}/Å^2/s$. The video shows nucleation and crystal growth under continuous electron beam irradiation.

1.5. Assessing growth rates

Video S11. Under prolonged electron beam irradiation at an electron flux of 10 $e^{-}/Å^2/s$, the initially formed FFA crystals in the 20 mM FFA solution in IPA exhibit structural degradation, likely due to solvent displacement and the limited beam resilience of the solvent. This observation highlights the importance of carefully controlling the exposure time during LPTEM experiments to preserve crystal integrity and obtain reliable structural information.

S7. Automated Growth rates

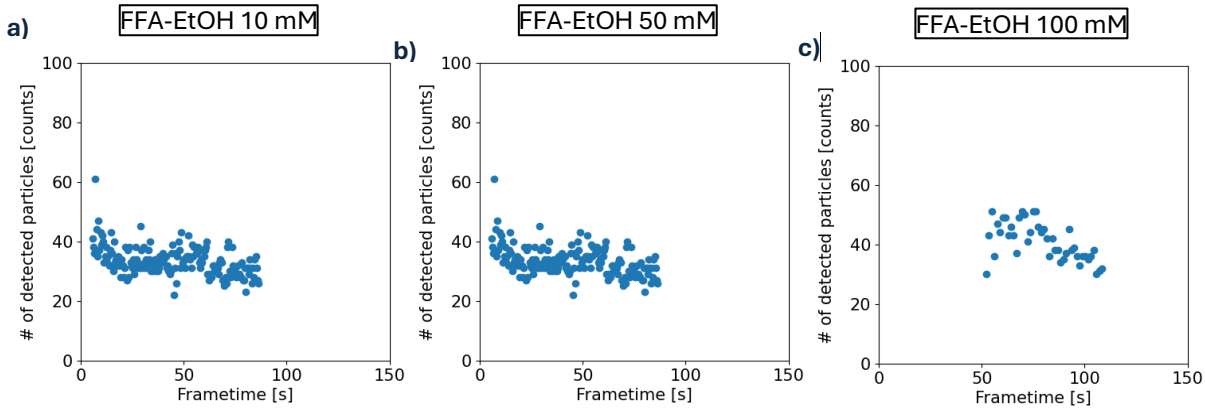

Figure S3. Number of detected particles via automated particle detection of FFA-EtOH (a) 10 mM, (b) 50 mM and (c)100 mM.

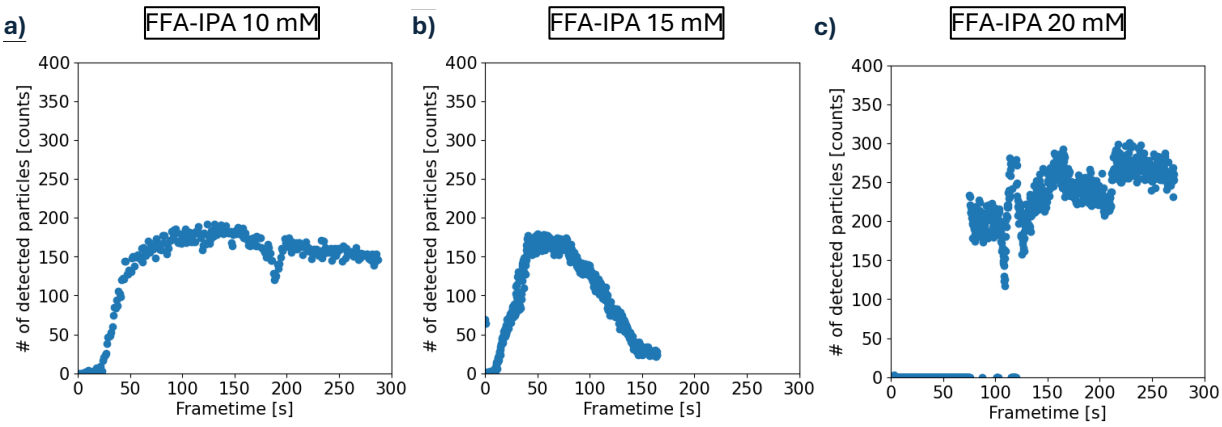

Figure S4. (a-c) Number of detected particles via automated particle detection of FFA-IPA 10, 15, 20 mM.

S8. Manual growth rates

1.6. Methodology for manual measurement of growth rate

For the growth rate of crystals to be analysed, 20 crystals were selected per frame, and size (width and length) was manually measured at 10-second intervals using Digital Micrograph (Gatan Microscopy Suite, GMS 3). The measurements were made retrospectively, beginning in the last frame where the crystals were detectable and working backward to their first detectable appearance to measure the onset of growth precisely. The size data gathered were plotted on Origin to produce growth curves. The growth rate of a crystal was determined from using the slope (m) of the linear fit from the equation $y = mx + c$. The final reported growth rate is the average of the individual slopes calculated for all 20 crystals in one set of data.

1.7. Results for manual growth rate

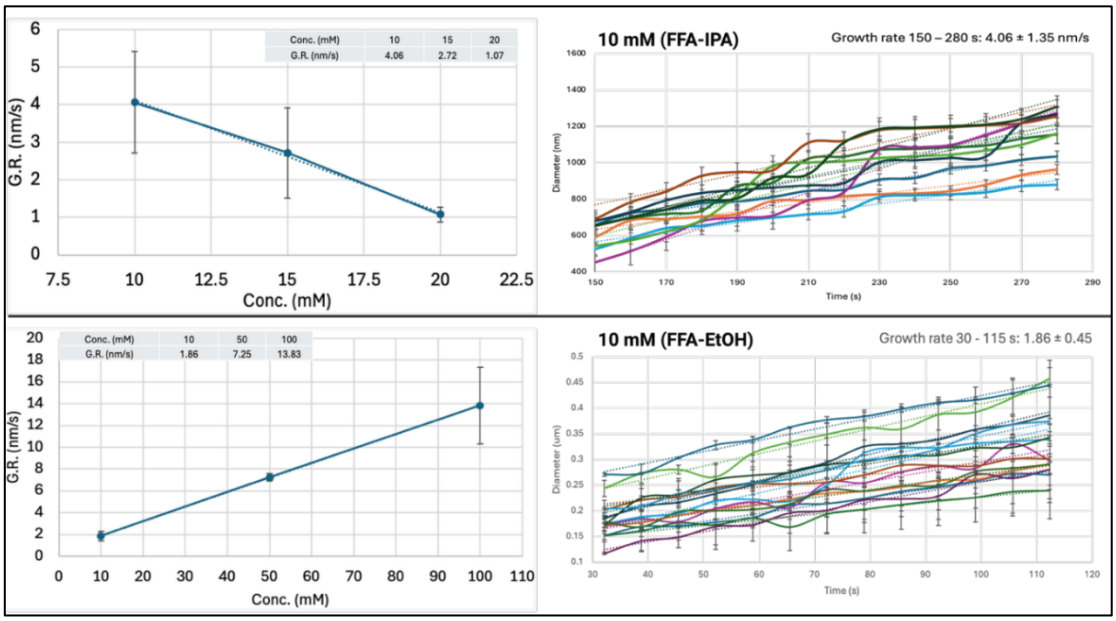

Figure S5. Manual growth rates in both the systems, FFA-IPA (top) and FFA-EtOH (bottom). (n=3)

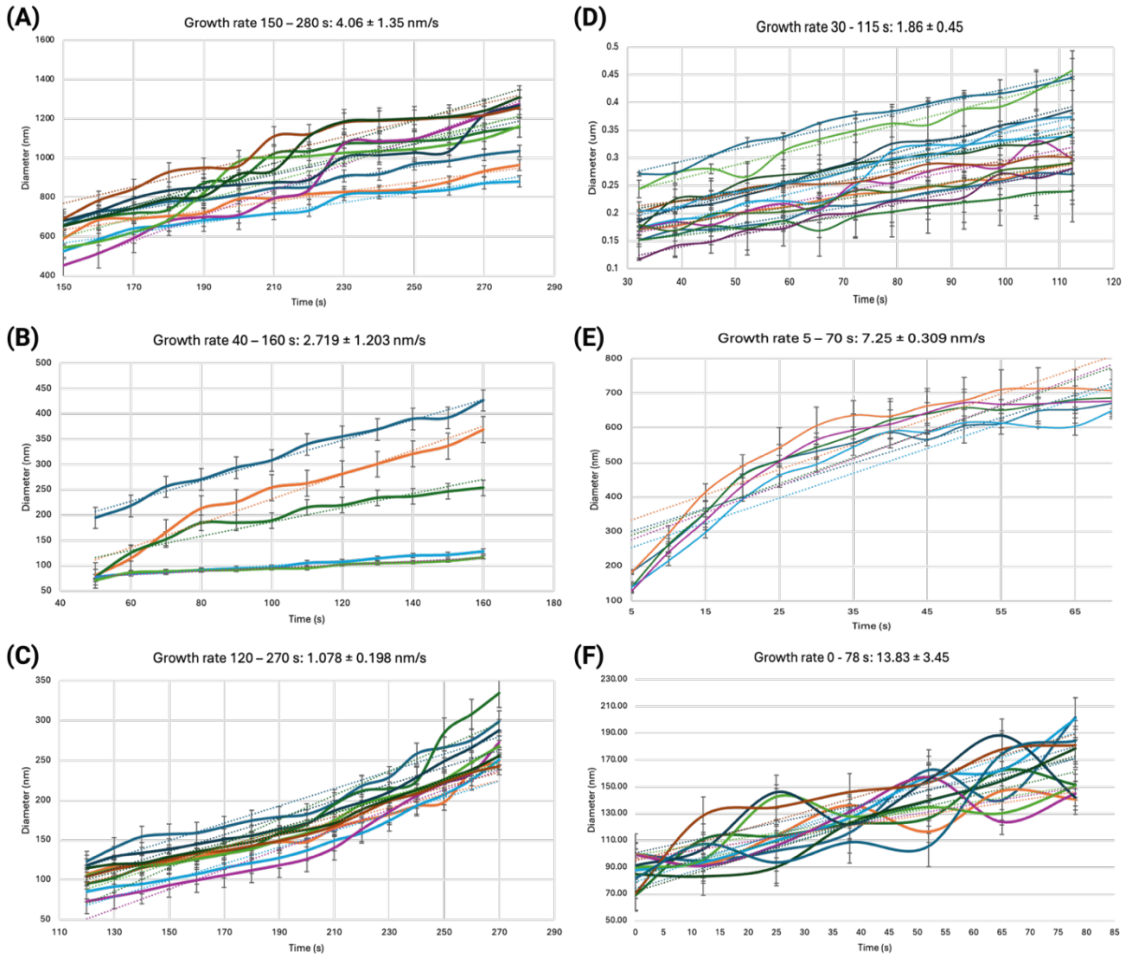

Figure S6. Manual growth rates, A to C (left) ~ FFA-IPA: 10, 15 and 20 mM; D to F (right) ~ FFA-EtOH: 10, 50 and 100 mM. All the concentrations showed a linear trend. (n=3)